On the critical amplitude in oscillating rolling element bearings

Fabian Schwack [a,b,*,1], Volker Schneider [b], Sebastian Wandel [b], Román José de la Presilla [a], Gerhard Poll [b], Sergei Glavatskih [a,c,d]

[a] *KTH Royal Institute of Technology, Department of Machine Design, SE-10044 Stockholm, Sweden*
[b] *Leibniz University Hannover, Institute of Machine Design and Tribology, DE-30167 Hanover, Germany*
[c] *Ghent University, Department of Electromechanical, Systems and Metal Engineering, B-9052 Ghent, Belgium*
[d] *University of New South Wales, School of Chemistry, UNSW, Sydney, NSW 2052, Australia*

ARTICLE INFO

ABSTRACT

Small oscillating amplitudes ($\sim 0.1°$) and larger ($> 1°$) can both lead to wear, which complicates the evaluation of the operating conditions. In this work, a simulation model is used to discuss critical amplitudes. The parametric study, which includes 125 simulations, shows the effect of load andcoefficient of friction on the frictional work density for amplitudes ranging from 0.1 to 2.5°. The study concludes that the frictional work density increases with the oscillating amplitude up to a certain point, where it becomes almost constant in relation to the amplitude. This point is reached when the amplitude is so large that a continuous overlapping of the contact zone no longer occurs. It is precisely this point that marks the critical oscillation amplitude.

1. Introduction

Oscillating bearings can be found in different industrial applications. The reciprocating motion between rolling element and raceway can lead to wear [1], which can occur in different forms [2,3]. A distinction between bad (wear) and good operating conditions (no wear) is often made using the oscillating amplitude. Therefore, the critical amplitude is the amplitude from which an increased amount of wear can be expected.

For fretting-contacts, exposed to pure linear sliding, those attempts were successful and led to fretting-maps [4], which allow classification of operating conditions under defined parameters. Such mapping is more difficult for rolling element bearings due to the complex kinematics and a combination of rolling and sliding. Nevertheless, simplified conditions (constant coefficient of friction μ) in the rolling bearing contact can be investigated with the help of simulation models. Although the conditions are simplified, the results can be clearly interpreted due to the lack of statistical deviations.

Bearings in the industry need to withstand very differently oscillating amplitudes. Oscillations can occur intentional (adjustment) or unintentional (vibration). Some examples are shown in Fig. 1. Examples for adjustment application can be found in space applications like antenna pointing mechanisms [5], heavy machinery like cranes [6,

7] or in constant velocity joints of cars [8,9]. Unintentional oscillations are very common since every machine component is affected in some way by vibrations. Documented bearing failure cases due to vibrations can be found in textile machines, in which the vibration of other machines in the same factory lead to wear [10], spindle bearings of a hammering machining tools [11], railway bearings [12] and, wheel-bearings that suffer from vibrations during shipping [13].

A popular example in which intentional and unintentional oscillation can occur are the pitch bearings of wind turbines [14]. The pitch bearing is used to adjust the blades to the current wind speeds [15,16]. If the turbine is at a standstill, due to low wind speeds or maintenance, the vibrations of the blade are transmitted into the bearing and lead to unintentional, small oscillations.

Due to the very different applications in which oscillating bearings are used, the focus of oscillating bearing research is often very diverse as well. For example, various operating conditions, bearing types, materials and lubricants are examined. To give the reader an overview of the current state of research, taking into account the various applications and different focuses, we have compiled a summary in Section 2.

In this work, we mainly focus on simulations to get detailed information for a large variety of oscillating amplitudes. With the help of contact simulations, the impact of the oscillating amplitude on frictional work density and wear is shown. This is done by using a simulation model, which was previously compared to experimental results by Schwack et al.

---

* Corresponding author.
  E-mail address: schwack@kth.se (F. Schwack).
[1] ORCID(s): 0000-0003-2581-9672

<table>
<tr><td colspan="2">Nomenclature</td></tr>
</table>

Greek Symbols

α	Contact angle
γ	$\frac{2 \cdot r_{RE} \cos\alpha}{d_m}$
δ_k	Displacement of point k
$\Delta\Phi$	Twist of rings per calculation step
θ	Double oscillating amplitude
μ	Coefficient of friction
ω	Angular velocity
ω_C	Angular velocity of rolling element center point
ω_{IR}	Product of angular velocity of inner ring
ω_{OR}	Product of angular velocity of outer ring

Roman Symbols

a	Length of the Hertz'ian contact area
a^*	Position of the line of pure rolling
A	Contact area
b	Width of the Hertz'ian contact area
d	Inner diameter
d_m	Pitch diameter of bearing
D	Outer diameter
f	Oscillating frequency
F_C	Normal contact load
FE	Finite Element
i_E	Element number in y-direction
j_E	Element number in x-direction
N	Cycles

P	Hertz'ian pressure
P_{IR}	Hertz'ian pressure inner ring
P_{OR}	Hertz'ian pressure outer ring
u^E	Element displacement
$u^E_{\Delta\Phi}$	Sliding path per change of angle
$u^E_{\Delta T}$	Absolute sliding path
$u^E_{C\Delta T}$	Relative sliding path diagonally to rolling direction (crosswise)
$u^E_{L\Delta T}$	Relative sliding path in rolling direction (lenghtwise)
u^n	Node displacement
r	Axis of rotation of the bearing geometry
r'	Distance to center of rotation
r_C	Radius of contact center point
$r_{i,o}$	Distances of the contact centers to the bearing axis of rotation
r_{RE}	Radius of rolling element
S_{diff}	Differential slip
T_S	Calculation steps
u_v	Sliding velocity
v_C	Velocity of rolling element center point
v_r	Rolling element velocity
v_{IR}	Tangential velocity of inner ring
v_{OR}	Tangential velocity of outer ring
W	Frictional work density
x	Travelled distance of the rolling element
Z	Number of rolling elements

[17]. The work aims to deeper understand the origin and distribution of sliding in oscillating contacts. The results are discussed regarding the adjustment of the operating conditions. Since the oscillation amplitude is the easiest to change in an actual application, the focus is placed on this parameter. The oscillating amplitude is analysed in 0.1° steps from 0.1° to 2.5° for five different parameter combinations (including load and coefficient of friction variations). This leads to 125 simulations overall. All simulations are applied to an angular contact ball bearing. The parametric study aims to clarify whether it is possible to derive a critical oscillation amplitude under simplified conditions, including a constant coefficient of friction for the entire operating time and smooth surfaces.

The state of the art (Section 2) of oscillating bearings will be briefly shown, and the different sliding components that occur in ball bearings will be derived by easy equations and assumptions (Section 3), which contribute to a better understanding of the contact mechanics. To assure the comparison to other bearing types, the non-dimensional parameter e will be explained and used in this paper (Section 4). The focus of the central part is on the design and the boundary conditions of the simulation model (Section 5) and the parametric study (Section 6) as well as the evaluation and interpretation of the results (Section 7).

2. State of the art

This section summarizes research on oscillating bearings as well as strategies to prevent wear. Furthermore, a brief overview of simulation models for oscillating bearing contacts is given.
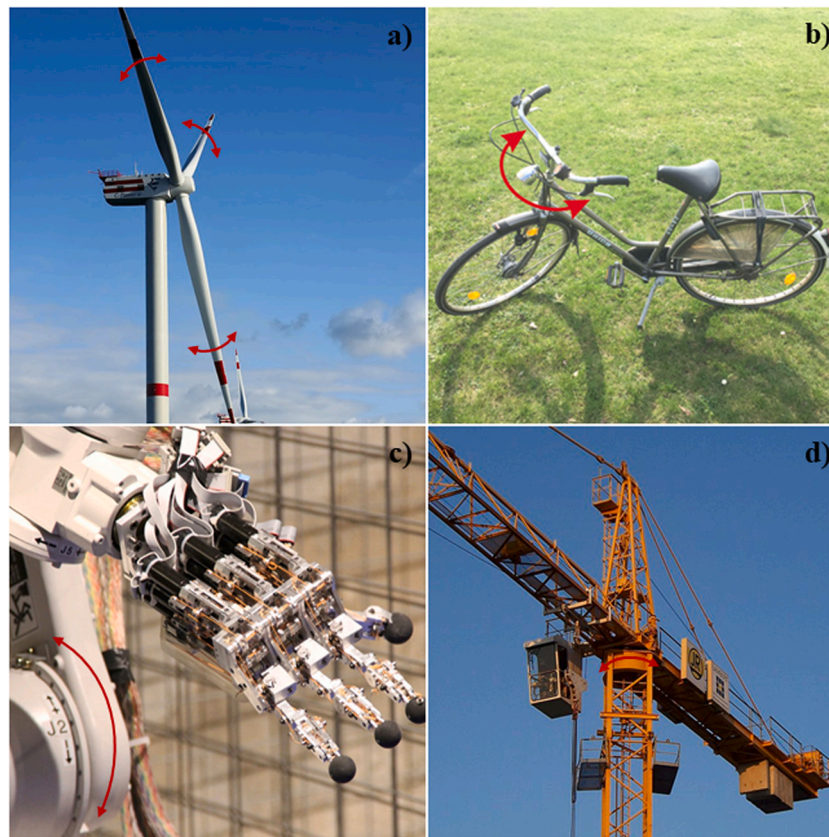
2.1. Wear in oscillating bearings

Fundamental investigations on wear in oscillating contacts are often based on fretting experiments, focusing on a single contact under pure reciprocating sliding. This approach allows experimental investigation in a very controlled environment that cannot reproduce the complex kinematics of rolling element bearings. The main difference is that

contacts in rolling bearings function under a mixture of rolling and sliding (rolling is mostly dominating). Furthermore, the sliding does not occur only in one direction. Due to the contact geometry, a complex superposition of different sliding components occurs, dominated by the spin and differential components (further details in Section 3).

Furthermore, the oscillating wear mechanisms are a complex interplay of kinematic and tribochemical effects. Operating conditions, lubricants and wear degradation heavily affect the type and degree of wear effects. The main wear mechanisms in oscillating bearings are False Brinelling and Fretting Corrosion. False Brinelling and Fretting Corrosion can occur under similar conditions if the oscillation amplitude is so small that slip occurs in a fixed contact region [18]. If the lubricant was squeezed out of the contact zone [19,20] or the lubricant was not able to separate the contacting surfaces [21,22] or if no lubricant was used, Fretting Corrosion likely occurs. While False Brinelling triggers mild adhesive wear, the surfaces are heavily stressed by Fretting Corrosion. With increasing oscillating amplitudes, the possibility of lubricant film establishment increases. If the surfaces are not separated for large amplitudes, wear occurs in the form of Fretting Corrosion, and leads to severe surface damages and often to particles that promote strong abrasive wear. Examples of the described damage mechanisms can be found in Fig. 2. In order to use oscillating bearings effectively in industry, various preventive measures can be used with regard to the design, the lubricant and the adaptation of operating conditions.

Various publications have dealt with wear in oscillating rolling bearings. The results cover a great variety of bearings types, operational conditions and lubricants. The work of Grebe and Schadow focused on the lubrication of rolling element bearings that are affected by very small oscillations (quasi-standstill [23] or vibrations) [18,23–27]. The research goes back to the first studies on False Brinelling by Almen [13]. The term False Brinelling is derived from the Brinell-hardness test [28], due to the somewhat similar visual appearance of the wear marks and marks from the hardness-test.

Fig. 1. Examples of oscillating bearings in industrial applications. Arrows are added to the original sources. a) Wind turbine pitch bearing b) Steering-bar c) Robotic application d) Tower crane bearing. Creative commons: a) CC BY-SA 4.0 HANS HILLEWAERT b) CC0 1.0 FABIAN SCHWACK c) CC BY-SA 3.0 LIONEL ALLORGE d) CC BY 3.0 DE HIGH CONTRAST. (For interpretation of the references to colour in this figure legend, the reader is referred to the web version of this article.)
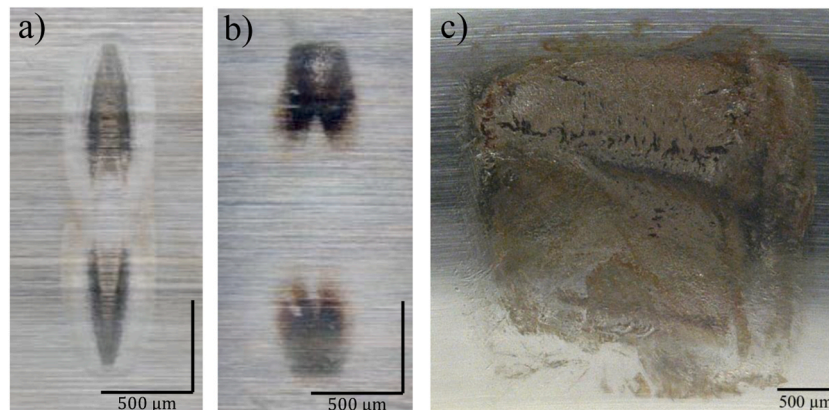
Fig. 2. Damage in oscillating bearings (7208). a) False Brinelling - lubricated with mineral oil (base oil viscosiy 100 mm^2). b) and c) Fretting Corrosion - dry and grease lubricated. Test conditions for a) and b) - $\theta = 1.0°$; $N = 25.000$ and $P = 1.9$ GPa. [22]. Test conditions for c) $\theta = 18.7°$; $N = 250.000$ and $P = 1.9$ GPa.

2.2. Wear prevention

To prevent wear caused by oscillating motion, various approaches can be pursued. As part of the state of the art, we briefly describe the possibilities for changing the bearing design, lubrication and operating conditions.

2.2.1. Design

The design of bearing used under oscillating is versatile and depends heavily on the installation conditions, which is why the design options are only briefly covered. In general, sliding bearings are an option [29, 30]. For some applications, sliding bearings are not an option since frequent start-stops are necessary and/or hydraulic systems are not
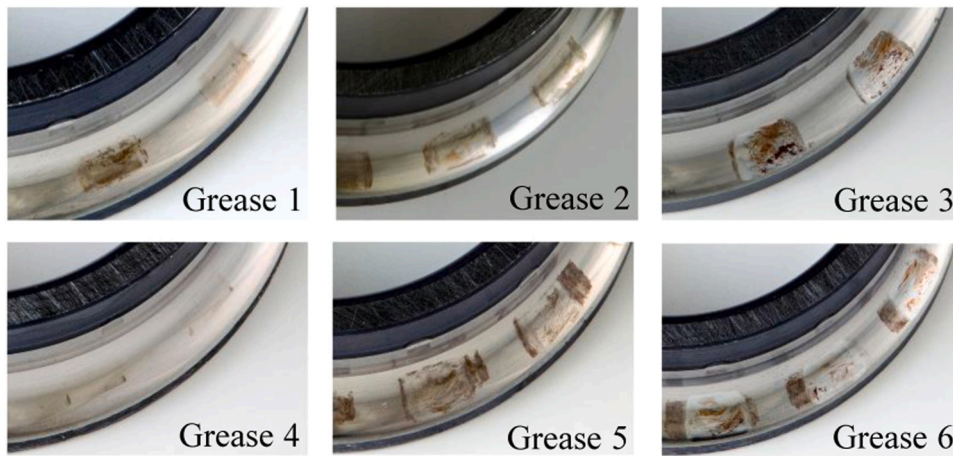
Fig. 3. Overview of grease test results from Schwack et al. [22]. Experiment parameters: bearing size 7208; $P_{IR} = 1.9$ GPa; $\theta = 18.7°$; $f = 5$ Hz and $N = 250,000$.

viable. Rolling element bearings can be improved by the use of coatings [31–34]. Since coatings involve additional costs, this option is not considered for some applications. Furthermore, the bearing design can be adapted to the application by using an improved arrangement of the rolling elements [35] or using new design approaches [36].

2.2.2. Lubricants

Proper lubricants are a proven concept to reduce wear in oscillating applications. Besides, the lubricant can usually be exchanged quickly and adapted in problematic applications. Experimental investigations for different operating conditions, different industrial applications and different oil and grease types were carried out in the past [18,21,22,27, 37]. The first publication on False Brinelling from 1937 contains experimental results for 40 different lubricants [13]. Almen concludes from the experiments that lubricants with low viscosity can not prevent but at least reduce False Brinelling, which is in line with modern literature [18,22,27].

The strong influence of different grease lubricants in oscillating applications was shown in Schwack et al. demonstrated for wind turbine pitch bearings [22]. Fig. 3 shows some results of the mentioned study.

2.2.3. Operational conditions

Tailored bearing design and proper lubricants in oscillating applications are undoubtedly necessary for a functioning application. In some cases, wear can not be prevented by changing the design or the lubricant. Therefore, it is essential to understand which of the operational conditions can be critical. For rolling element bearings, equations for critical oscillating amplitudes can be found in Harris et al. [35]. The critical amplitude θ_{crit} is defined as the angle of rotation of the inner raceway relative to the outer raceway for which a raceway portion is only stressed by one rolling element.

$$\theta_{crit} = \frac{720°}{Z(\mp\gamma)} \tag{1}$$

According to Harris et al. wear likely occurs for amplitudes smaller than the half of θ_{crit}. The definition of θ_{crit} is only a rough guide since the reduction of rolling elements Z under the same contact conditions will not affect wear.

$$\theta < \theta_{crit}/2 \tag{2}$$

Another amplitude defined by Harris et al. is θ_{dith}. For θ_{dith} the oscillating amplitude is smaller than the width of the contact $2b$. According to Harris et al. Fretting Corrosion likely occur under that conditions.

$$\theta_{dith} = \frac{720°\cdot b}{\pi d_m(1 \mp \gamma)} \tag{3}$$
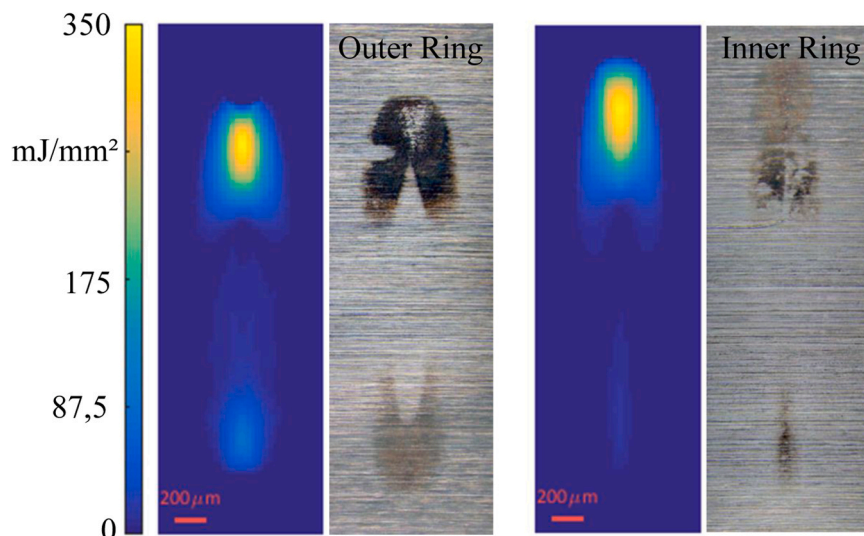

Fig. 4. Comparison of experiment and simulated frictional work density from Schwack et al.[17].

2.3. Simulation of oscillating bearings

The presented research is based on the contact model published in 2018 [17]. The model simulates a ball between two raceway segments in an oscillating bearing. The results are pressure, sliding path (relative accumulated displacements) and frictional work density. Similar models can be found in McColl et al. [38], Schadow et al. [27], Fallahnezhad et al. [12,39,40] and Cubillas et al. [41]. The main difference of our simulation model is the possibility to perform parametric studies, since all parameters can be changed, and the mesh adapts automatically.

Fig. 4 shows a comparison of simulation and experiments for a angular contact ball bearing 7208 [22]. The correlation between frictional work density and wear [42] can be clearly seen. Similar simulations and experiments were also performed for fretting contacts [43–45].

3. Ball motion and relative displacements

In order to understand the wear mechanisms, the bearing kinematics must be understood. Therefore, a short introduction into ball motion and sliding path (relative accumulated displacements) in the contact will be given by simplified equations. The deviation of the speeds in the friction contact is referred as slip and has an influence on the wear behaviour. The kinematic conditions and the resulting sliding in the angular contact ball bearing are derived below.

More advanced and complex equations can be found in Jones [46] or for four-point contact ball bearing, which behaves similar to angular contact ball bearings, in Leblanc and Nelias [47] or more general in Johnsson [48].

3.1. Kinematics

Assuming a point contact and no relative movement of the contact points and no elastic deformation of the components involved, simplified equations for describing the kinematic relationships can be derived. The following assumptions are idealized.

The tangential velocities v_{OR} (outer ring) and v_{IR} (inner ring) result from the product of the angular velocities ω and the rotary axis distances r.

$$v_{OR} = \omega_{OR} \cdot r_o \tag{4}$$

$$v_{IR} = \omega_{IR} \cdot r_i \tag{5}$$

The velocity of the rolling element center point v_C and ω_C can be calculated due to the proportional behaviour of the velocity vectors.

The velocity of the center of the rolling element v_C and ω_C can be calculated from their mean values on the basis of the proportionality of the velocity vectors.

$$v_C = \frac{\omega_{OR} \cdot r_o + \omega_{IR} \cdot r_i}{2} \tag{6}$$

$$\omega_C = \frac{\omega_{OR} \cdot r_o + \omega_{IR} \cdot r_i}{2 \cdot r_C} \tag{7}$$

The distances of the contact centers to the bearing axis of rotation r_i and r_o can be determined with the radius of the rolling element centers r_C, the rolling element radius r_{RE} and the contact angle α.

$$r_o, r_i = r_C \pm \cos(\alpha) \cdot r_{RE} \tag{8}$$

With the help of this equation, the relative rolling velocity v_r can be calculated by substitution.

$$v_r = (\omega_{OR} - \omega_{RE}) \cdot r_o \tag{9}$$

$$v_r = \frac{(\omega_{OR} - \omega_{IR}) \cdot (r_C^2 - (r_{RE}^2 \cdot \cos^2(\alpha)))}{2 \cdot r_C} \tag{10}$$

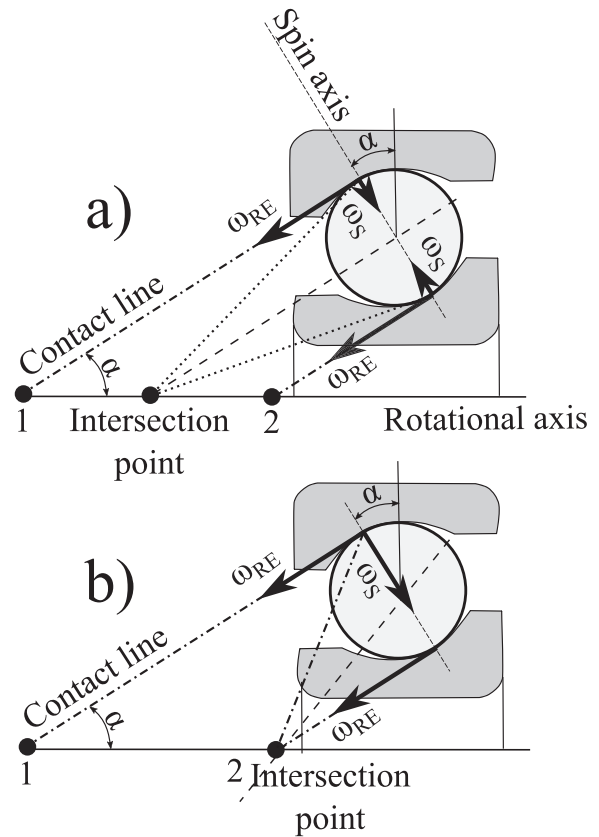All rolling points must have an identical velocity. The center of

Fig. 5. Schematic representation of the spin slip for a rolling element of an angular contact ball bearing when a) the slip on both raceways is the same and b) the slip only occurs on the outer raceway.

gravity of the rolling element rotates with the angular velocity ω_C. Hence ω is a relative velocity in the coordinate system rotating with the angular velocity of the rolling element ω_C, see Fig. 5. On the basis of these kinematic conditions, the sliding in different bearing types can now be derived.

$$\omega = \frac{v_r}{r_{RE}} = \frac{(\omega_{OR} - \omega_{IR}) \cdot (r_C^2 - (r_{RE}^2 \cdot \cos^2(\alpha)))}{2 \cdot r_C \cdot r_{RE}} \tag{11}$$

3.2. Sliding

In real conditions, the rolling process always consists of a combination of rolling and sliding movement in the contact. The deviation between the described ideal conditions and the actual conditions, which result from the superimposed sliding movement, is called slip.

Thus, the sliding velocity u_v of two coinciding points between the two contact partners results from the displacement of the point in space δ_c and its time derivative.

$$u_v = \frac{\Delta \delta_c}{\delta_t} \tag{12}$$

3.2.1. Spin component

For ball bearings with a contact angle $\alpha > 0°$, spin slip occurs. Fig. 5a shows a section view of an angular contact ball bearing with the contact angle α. Due to the balance of forces, the contact points of the inner and outer ring must be opposite each other. The tangents intersect the bearing axis of rotation at points 1 and 2. The rolling element rotates with the angular velocity ω relative in the coordinate system rotating with the angular velocity of the rolling element ω_C.

Due to the contact angle α, two movements are superimposed. The ball rolls on the track at the velocity ω_R (rolling movement). At the same
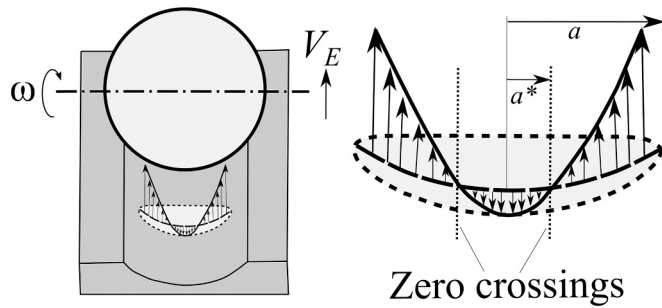
Fig. 6. Schematic representation of the differential slip for a rolling element of a ball bearing. The dashed lines represent the contact area. In the shown velocity profile the point with zero slip are marked. The velocity profile is purely schematic.

Fig. 7. Different *e*-ratios for better representation. Typical *e*-ratios for wind turbine pitch bearings can be found in Schwack et al. [22] and Stammler et al. [53].

time, the ball and the track rotate against each other around an axis perpendicular to the normal contact surface. The overlapping of both forms of motion intersect the rolling element and bearing axis of rotation. In the schematic representation in Fig. 5a it is assumed in a simplified manner that only spin slip occurs and that the slip for the inner and outer ring have equal values. As a result, the axis of rotation of the spin slip is orthogonal to the axis of rotation of the rolling element.

The distribution of the spinning components between the inner ring and outer ring is largely determined by the contact area *A* and the coefficient of friction *μ* (as shown later). If, for example, the contact area on the inner ring becomes longer than on the outer ring, more slip will occur on the outer ring due to the contact conditions. At very high velocities, the centrifugal force of the rolling element leads to larger contact areas on the outer ring, which causes more slip on the inner ring. As a rule, the raceway curvatures of the inner and outer rings are chosen so that the pressure distributes as even over both raceways.

If the macro geometry of the raceways or the surface roughness is changed (e.g. due to wear), this also impacts slip distribution for both raceways. A change in the geometry results in a change of *μ*, which influences the slip. Fig. 5b schematically shows the case of the spin slip occurs on the outer ring only. This results in an inclination of the spin turning axis. The intersection of rolling element and bearing axis of rotation shifts in comparison to Fig. 5a towards the radial plane and falls into point 2. At the ends of the contact ellipse with the greater distances from the bearing axis of rotation, the direction of the sliding movement due to the spin torque is identical to the direction of the rolling movement.

3.2.2. Differential component

The surface of the Hertz'ian contact area under the influence of a load has a curvature due to their deflection. This results in differential slip along the contact surface, which results from the circumstance that every point in the contact area has a different radius to their spinning axis. This differential slip is often called Heathcote-slip [49]. Generally, the velocity at any point $u(x, y)$ is the product of the effective angular velocity ω in the contact and its distance to the center of rotation $r'(x,y)$.

$$u(x, y) = \omega \cdot r'(x, y) \qquad (13)$$

In the contact area, the slip is basically divided into an area with differential speed along the rolling direction and another against the rolling direction. This would accordingly lead to two lines within the contact in which pure rolling occurs. To calculate the position of the line of pure rolling, an approximation was defined in [50,51].

$$a^* = 0.347 \cdot a \qquad (14)$$

Fig. 6 shows schematically the distribution of the differential slip in a ball bearing. The rolling velocity v_w lies between the circumferential speed at the largest r'_2 and the circumferential speed at the smallest radius r'_1. Consequently, the direction of the relative movement, which
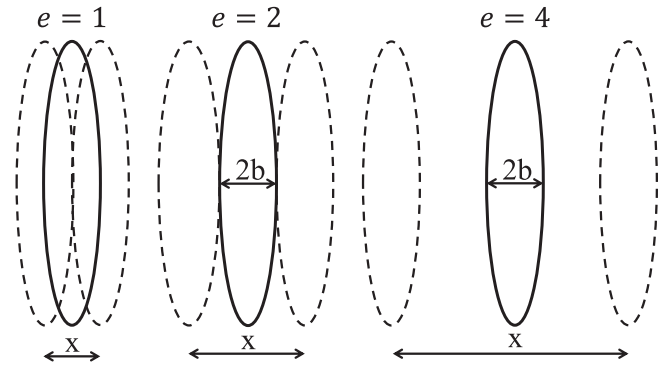
represents the slip at the smallest radius, is identical to the rolling movement ω. At the largest radius, the slip direction is opposite to the roll direction. The rolling velocity v_r results from the balance of the forces and torques that arise from the frictional forces in the contact zone.

3.2.3. Elastic component

If an elastic ball (convex) is pressed onto a curved elastic raceway (concave), the resulting elastic deformations cause distortions on both surfaces. In the example of the ball bearing, the surface of the raceway stretches while the surface of the ball compresses. This creates a relative movement which represents the slip due to elastic deformations. If there is a loosening, there are again relative movements that show opposite directions compared to the previous example.

4. Dimensionless oscillating parameter *e*

To make the results scaleable to different bearings sizes, the dimensionless parameter *e* will be used, which is based on the rolling element movement distance *x* in relation to the contact width 2*b*, defined by Hertz [52].

$$e = x/2b \qquad (15)$$

Fig. 7 shows different *e* ratios. The ellipse in the center shows the Hertz'ian contact ellipse and the dashed lines the movement distance.

Equal dimensionless parameters were used in the literature on oscillating bearings [16,22] and also in literature that investigates single contact behaviour [37,44]. Therefore, the presented results can also be compared with literature that investigated different sizes of *e*.

5. Simulation model

The shown derivation of slip components in an angular ball bearing was carried out taking into account some simplifications, such as a predetermined distribution of the sliding components between the inner and outer ring and a contact angle that corresponds to the nominal contact angle. In addition, an analytical calculation of the sliding would require considerable time for the desired investigations, since the slip needs to be calculated for different positions on ball and raceway. Computing the slip directions in particular is associated with complex coordinate transformations. Therefore a FE-Model is used to calculate pressure, sliding path and sliding directions. In order to obtain realistic calculation times, the model is not transient. The physics of the simulation environment (ANSYS [54]) were used in the model.

The model simulates the rolling element of a bearing between two raceway segments. One contact is between the rolling element and inner ring segment and another contact is between the rolling element and outer ring segment. The schematic structure of the model can be seen in Fig. 8.
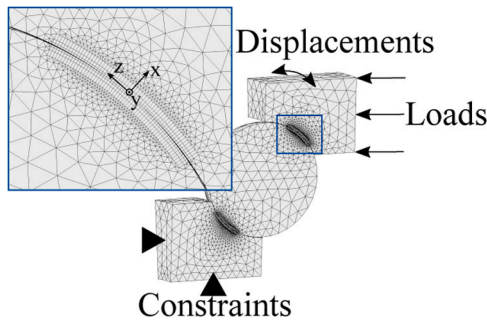
Fig. 8. Schematic representation of model and mesh in the contact zone. For better visibility in schematic representation, the density of the mesh and the volume of the fine meshed area has been reduced.

The movement of the rolling element is determined by the geometry of the raceway and rolling element, the load and the fixed coefficient of friction. This enables the analysis of the sliding path in the contact zone that occurs due to the oscillating movement.

The model is fully parametric and the mesh automatically adapts to the contact conditions, to ensure that all stresses occur within the fine mesh. This enables the analysis of various extensive parameter studies. The mesh of the model is shown in Fig. 8. A fine mesh is necessary in the contact area. Trilinear 8-node hexahedron elements are used for regular mesh. The weaknesses of this type of element occur with bending and incompressible materials. Bending and incompressible materials are not relevant for the desired simulations, so this element type allows a higher resolution and faster calculation times compared to higher-order element types. The same element type is used as a tetrahedral 4-node element in the support structure. In addition, surface elements are used in the contact area for finding contacts. With the help of multi-point constraints, the connection of several nodes can be established. During the oscillation, the relative displacements between the nodes can be calculated, which corresponds to the sliding path in the rolling bearing. In addition, the mesh allows both the size and the direction of the sliding path to be calculated at any position in the contact. The local pressures can also be determined.

The selected mesh and mesh fineness are based on a detailed mesh study. The greater the oscillating amplitudes, the greater the uncertainties that can occur from the mesh. In the mesh study, the focus was therefore placed on the fact that the uncertainties are less than 5% for large amplitudes. For small amplitudes, the uncertainties are therefore significantly smaller. Further uncertainties can occur due to the interaction of the raceways. For example, the shape of the contact ellipse and reaching $e = 1$ is different for inner and outer ring due to the different osculations.

The sliding path during the oscillation can be used to calculate the frictional work density W which is the product of sliding path u, coefficient of friction μ and contact pressure p. The local frictional work density describes the dissipated energy in the near surface depending on the friction and pressure of a finite surface. The assumption is made that the friction energy is transferred to the near surface without losses, for example heat.

$$W = \mu \cdot u \cdot p \tag{16}$$

The frictional work density W can be used as an indicator for wear [42], since frictional work and wear show a linear correlation. The correlation depends on the operating parameters and the tribological system. The main influencing parameters under dry conditions are the geometry of the contact partner, oscillating amplitude, coefficient of friction and pressure. Lubricated conditions contain further influencing parameters. However, such conditions can be approximated by an adjusted coefficient of friction. This publication is dedicated to the relative displacements that occur under different operating conditions. The correlation between frictional work and wear is not deepened.

The calculation of the sliding path is accomplished in several simulations steps, which can be chosen freely before the simulation. In Fig. 9 a schematic simulation with 14 steps is shown. For real simulations 20–48 steps are used for an sufficient resolution. The needed steps are dependent from the contact geometry, the operational parameters and the needed resolution.

The displacements of the nodes u^n are averaged for each of the 4 nodes of one element to calculate the average element displacement u^E. For the calculation i_E represents the element number in y-direction and j_E in z-direction.

$$u^E(i,j) = \sum_{i=i}^{i+1} \sum_{j=j}^{j+1} \frac{u^n(i,j)}{4} \tag{17}$$

The sliding movements must be calculated in and across the roll direction, in the local coordinate system. The relative displacements in the rolling direction are explained as examples. Transversely to the rolling direction, the z-components must be used instead of the y-components, see Fig. 8.

The displacements of the elements in the y direction are subtracted for two successive calculation steps T_S of the simulation. The resulting mean displacement per step T is subtracted from the shifts of the opposite elements. This leads to the relative displacement $u^E_{L\Delta T}$. The following equation can be used as an example for one element:

$$u^E_{L\Delta T} = u^E_{y,RE}(T) - u^E_{y,RE}(T+1) - ((u^E_{y,RW}(T) - u^E_{y,RW}(T+1))) \tag{18}$$

To calculate the accumulated sliding path u^E_L between any two steps, the amounts of the individual steps are added up. This allows the sliding path to be calculated during a full oscillation cycle. By dividing the rotation of the bearing rings $\Delta\Phi$, the sliding paths per angle change $u^E_{\Delta\Phi}$ can be calculated.
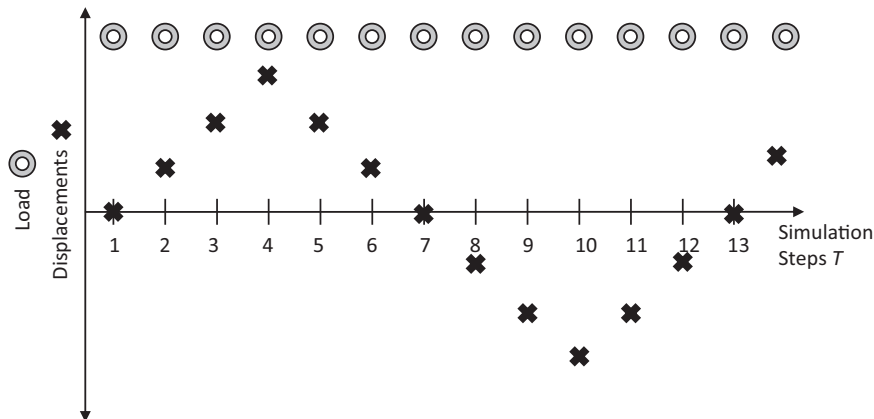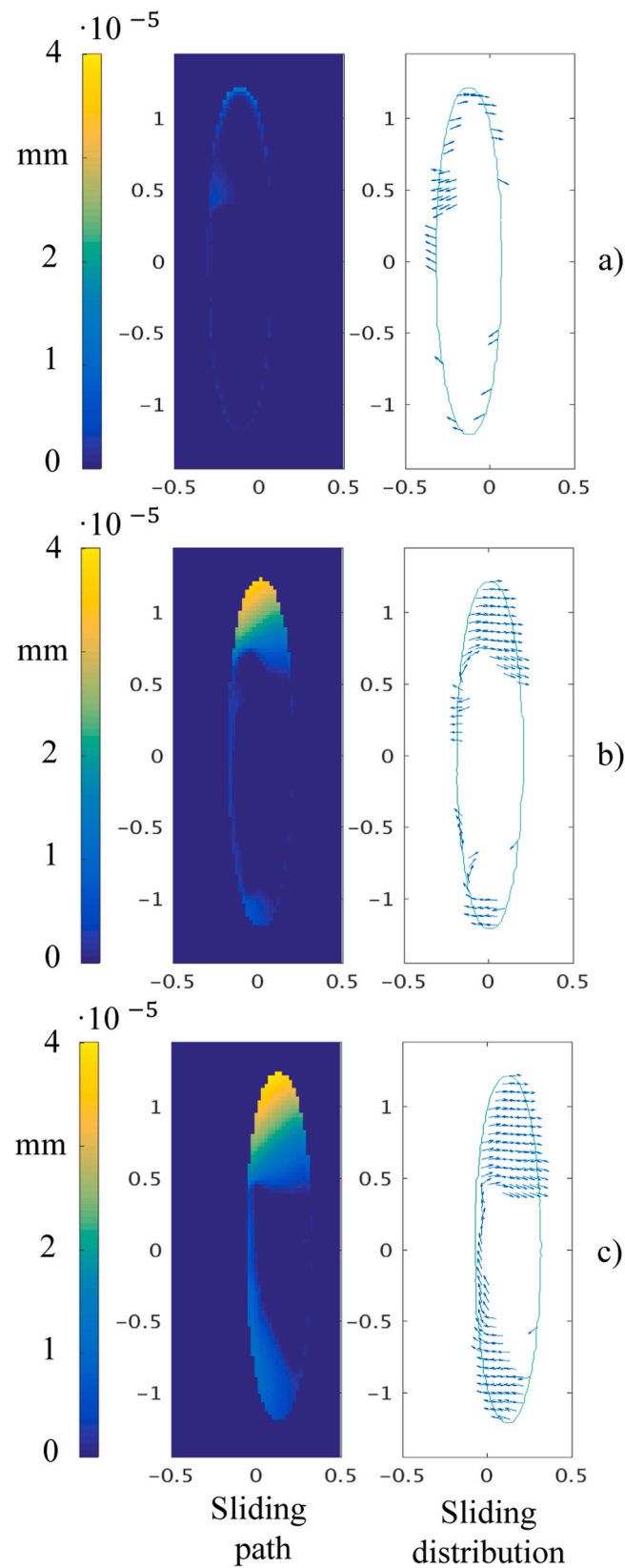

Fig. 9. Schematic representation of the simulation steps. A lower resolution of simulations steps was chosen for a better illustration.

Fig. 10. Overview of sliding path and sliding distribution for different positions during the oscillation. The columns a), b) and c) are the relevant positions during the oscillation. a) represents the position directly after the start of the oscillation or after the reversal point. b) is the zero crossing position and c) represents the position before the reversal point. For each position the sliding path in mm is shown in row 1 and the sliding distribution is shown in row 2.
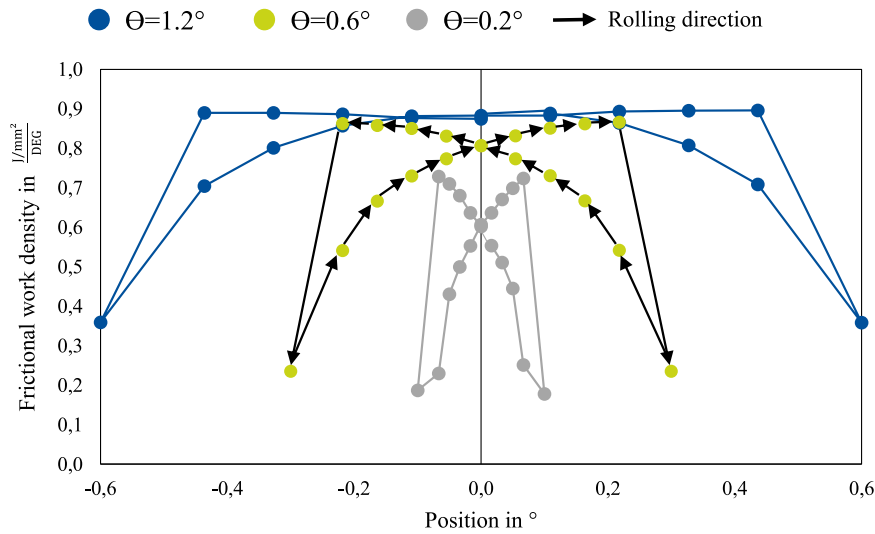
Fig. 11. Frictional work density per degree for an angular contact ball bearing and (P_{IR} = 1,76 GPa) at different positions of the oscillation. The simulations are performed with different double oscillation amplitudes of 0.2, 0.6 and 1.2°.

Table 1
Geometry of angular contact ball bearing 7208 (manufactured by FAG).

Outer diameter D	80 mm	
Inner diameter d	40 mm	
Rolling element radius r_{RE}	5.93 mm	
Contact angle α	40°	
	OR	**IR**
Osculation	93.8%	96.0%

The raceway radius and radius of the rolling element that are leading to the osculations were measured using a laser-scanning microscope.

Table 2
Chosen parameters for the study.

P_{IR}	P_{OR}	F_C	$e_{IR} = 1.0$	$e_{IR} = 1.5$	μ
2.05 GPa	2.00 GPa	1.27 kN	1.5°	2.2°	0.1
2.05 GPa	2.00 GPa	1.27 kN	1.5°	2.2°	0.2
1.76 GPa	1.71 GPa	0.79 kN	1.2°	1.9°	0.1
1.76 GPa	1.71 GPa	0.79 kN	1.2°	1.9°	0.2
2.79 GPa	2.72 GPa	3.17 kN	2.0°	3.0°	0.1

Including 125 simulations.

$$u_\Phi^E = \frac{u_{\Delta T}^E}{\Delta \Phi} \tag{19}$$

The absolute sliding path results from the geometric additions of the directional sliding movements in the rolling direction $u_{L\Delta T}^E$ (lenghtwise) and transverse to the roll direction $u_{C\Delta T}^E$ (crosswise).

$$u_{\Delta T}^E = \sqrt{{u_{L\Delta T}^E}^2 + {u_{C\Delta T}^E}^2} \tag{20}$$

5.1. Distribution of relative movements

As described in Schwack et al. [17], mainly the spin and differential slip impact the frictional work density. Relative movements from elastic deformation are comparable small [55]. For a better visualisation, a representation of the sliding path and the sliding distribution for 3 important positions of the oscillation are shown in Fig. 10. In the beginning of the oscillation only small relative movements occur. Anyhow, from the distribution, the typical superposition of spin and differential slip is already visible. In the upper and lower end of the ellipse the spin motion is visible, and in the middle the negative part of
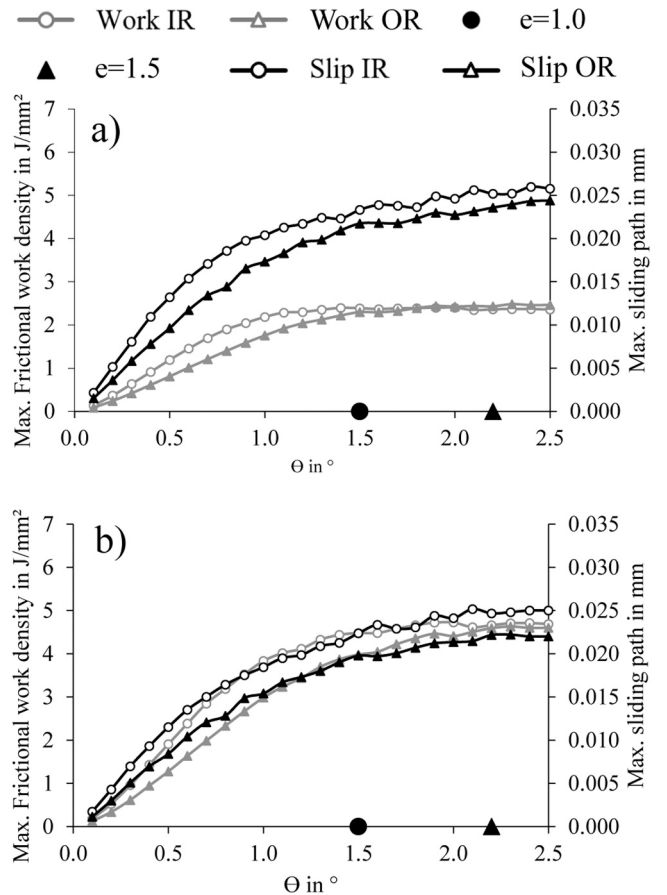

Fig. 12. Results for a) $\mu = 0.1$ and b) a) $\mu = 0.2$, $P_{IR} = 2.05$ GPa and $P_{OR} = 2.00$ GPa. $e = 1$ occurs at $\theta = 1,5°$ and $e = 1.5$ at $\theta = 2,2°$.

the differential component occurs. In the upper half of the ellipse the highest amount of slip occurs, since the spin and differential component share the same direction [17]. With increasing motion, this behaviour becomes more and more visible. The highest amount of sliding occurs before the end of the oscillating amplitude. After c) similar behaviour to a) will occur, with the difference that the direction will be the opposite. The described distribution of slip can be summed for a full oscillation,
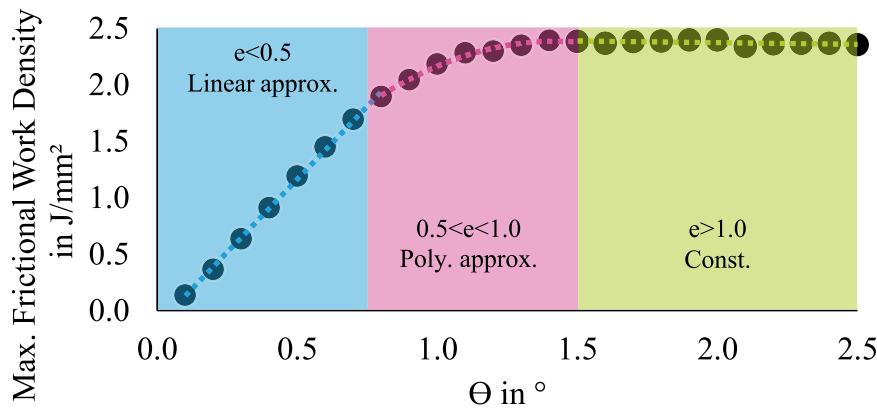
Fig. 13. Approximations for $\mu = 0.1$ and $P_{IR} = 2.05$ GPa. $e = 1$ occurs at $\theta = 1{,}5°$.

leading to the result which is shown in Fig. 4. The described behaviour needs to be kept in mind for the analysis of the slip and stick regimes.

6. Parametric study

The simulations are intended to clarify the question of whether a critical oscillation amplitude can be derived under simplified conditions. Therefore, variations of the oscillation amplitude are in the foreground of the parametric study. The need of a parametric study can be seen from simulation results which are shown in Fig. 11.

The plot shows frictional work density per 1° for an angular contact ball bearing and $P_{IR} = 1{,}76$ GPa at different positions of the oscillation, for 3 different oscillating amplitudes. Therefore, the outer points show the reversal points of the oscillation. For this simulations the double amplitudes were set to 0.2, 0.6 and 1.2°. The maximum frictional work density value for 0.2° is around 0.7 $\frac{J/mm^2}{1°}$. For 0.6° the behaviour is different due to the contact kinematics and a maximum value of around 0.9$\frac{J/mm^2}{1°}$ is reached. The last simulation with a double amplitude of 1.2° reaches values that are slightly higher than 0.9$\frac{J/mm^2}{1°}$ and shows a behaviour in which the frictional work density is constant.

On the basis of these simulations, the question arises whether the initially increase in the frictional work, which changes to a constant behavior with larger amplitudes, can be used to define a critical amplitude. To clarify this question, the level of detail in the simulations must be increased in order to better understand the behavior of the frictional work and the described transition from non-constant to constant frictional work. Furthermore we aim to clarify which approximated function can be used to describe the non-constant behaviour. The influence of the pressure and the coefficient of friction on the behavior described must also be taken into

account in the course of the parameter study.

To analyse this transition and the plateauing behaviour of the frictional work density in more detail, the maximum values of the frictional work densities for double oscillation amplitudes from 0.1° to 2.5° are simulated in 0.1° steps for various parameter combinations. This means that for every amplitude from 0.1° to 2.5°, 25 full simulations are completed. The bearing geometry can be found in Table 1. The simulation input is given in Table 2.

Simulations are completed with pressures P_{IR} of 2.05, 1.76 and 2.79 GPa. [56]. The corresponding contact normal loads F_C for one rolling element are listed in Table 2. Furthermore, simulations with $\mu = 0.1$ and 0.2 are accomplished. The amplitude that corresponds to $e = 1$ and $e = 1.5$ are also given in this table for each parameter combination. As explained before, describes e the travelled path of the rolling element in relation to the width of the Hertz'ian contact area. The parameter study comprises a total of 125 simulations which will provide more information about the behavior of the frictional work density as a function of the amplitude.

7. Results

According to literature, defined critical oscillating amplitudes occur at $e = 1$ (Eq. (3)) and at $e = 1.5$, under which no lubricant film will establish (Maruyama et al. [21,37]). Next to this, θ_{crit} (Eq. (1)) would occur for the test bearing at 51.42°, which is out of range for this investigations. The limits of $e = 1$ and $e = 1.5$ were already given in Table 2 and will be visualised in the Figs. 12–16.

Fig. 12a shows the maximum frictional work densities and the maximum relative displacements for the inner and outer ring. The pressure on the inner ring is 2.05 GPa and 2.00 GPa on the outer ring. For the inner ring applies, $e = 1$ for $\theta = 1.5°$ and $e = 1.5$ for $\theta = 2.2°$. The coefficient of friction is assumed to be $\mu = 0.1$. Due to the contact kinematics, the sliding path on the inner ring is somewhat larger than on the outer ring.

Up to a double oscillation amplitude of 1.4° this also applies to the frictional work density. For the inner ring, the constant behaviour of the frictional work occurs from approximately 1.1°. For the outer ring at around 1.4°. While the frictional work below 1.4° on the inner ring is greater due to the higher pressure, the frictional work density for 1.5° is very similar for the inner and outer ring. The reason for this is the equilibrium condition of the spin moments, which must apply to the contacts of the inner and outer ring. For $e > 1$, identical wear of both raceway contacts occurs. It becomes also clear, that only below $e > 1$ an increase of the frictional work occurs. For the maximum sliding path, the transition can also be seen but less pronounced compared to the frictional work density.

The analysis shows that the frictional work density does not change anymore for $e > 1$. However, between $e = 0.5$ and $e <= 1$, the frictional work density can be approximated with a second-order polynomial
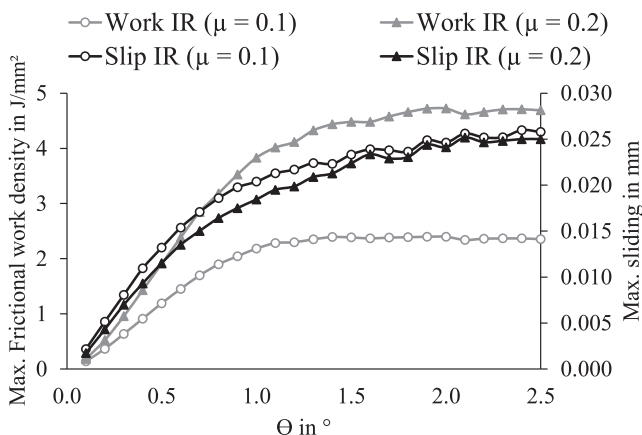

Fig. 14. Comparison of results for $\mu = 0.1$ and $\mu = 0.2$, Fig. 12a and 12b.
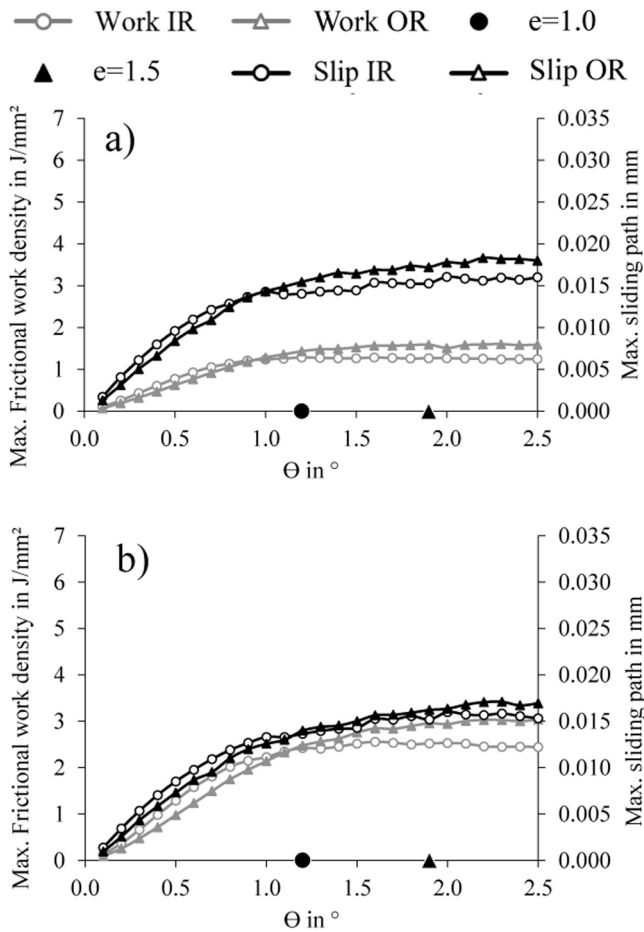
Fig. 16. Results for $\mu = 0.1$, $P_{IR} = 2.79$ GPa and $P_{OR} = 2.72$ GPa. $e = 1$ occurs at $\theta = 2.0°$ and $e = 1.5$ at $\theta = 3.0°$.

Fig. 15. Results for a) $\mu = 0.1$ and b) $\mu = 0.2$, $P_{IR} = 1.76$ GPa and $P_{OR} = 1.71$ GPa. $e = 1$ occurs at $\theta = 1.2°$ and $e = 1.5$ at $\theta = 1,9°$.

function. For $e < 0.5$, it is possible to approximate the frictional work with a linear function. Between $e = 0$ and $e < =1$ a polynomial function of second-order allows sufficient approximation. The approximations for $\mu = 0.1$ and $P_{IR} = 2.05$ are visualised in Fig. 13.

To investigate the impact of the coefficient of friction μ on the frictional work density, the same simulations are accomplished with $\mu = 0.2$. Fig. 12b shows the simulation results for a coefficient of friction of 0.2, $P_{IR} = 2.05$ and $P_{OR} = 2.00$. The sliding path is only slightly influenced by the coefficient of friction. The behaviour of the frictional work density changes. The value of the friction work density is doubled due to the coefficient of friction chosen twice. A similar transition of frictional work density and sliding is shown in 12a for $\mu = 0.1$ can also be found for $\mu = 0.2$ in Fig. 12b. A comparison of the results for $\mu = 0.1$ and $\mu = 0.2$ is shown in Fig. 14.

A change of the load also means a change of the kinematics since the pressure and the contact angle change. In Fig. 15a the pressure on the inner ring P_{IR} is 1.76 GPa and on the outer ring P_{OR} is 1.71 GPa. As already shown in Fig. 12, the sliding path at the beginning is larger on the inner ring. With 1.0° the sliding path on the outer ring becomes larger than on the inner ring. The reason for this is the inclination of the spin axis, which leads to greater sliding paths on the outer ring due to the lower load. The behaviour described can also be discovered for the frictional work density. The increase of the friction work density occurs up to approx. 0.8°. For the outer ring at around 1.1°. Again the transition occurs around $e = 1$. The same simulations are again be done for $\mu = 0.2$. Fig. 15b shows the results for a coefficient of friction of 0.2. The observations from Fig. 12 also apply to the lower load. The impact of μ on the sliding is negligible and the frictional work density increases by double the value.
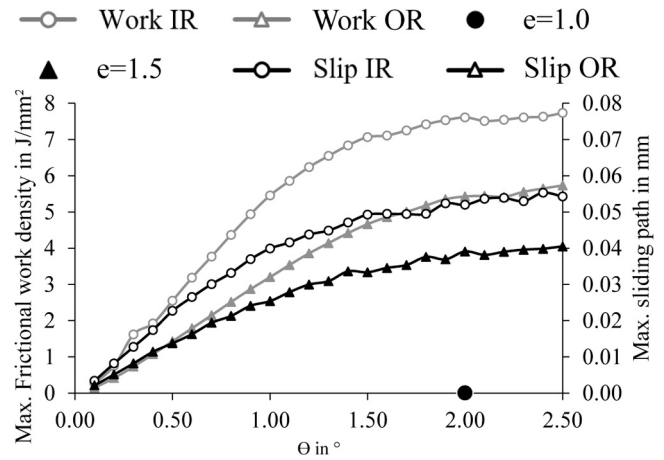
If the pressure of the inner ring P_{IR} is increased to 2.79 GPa, $e = 1$ on the inner ring corresponds to 2.0°. The simulation results can be seen in Fig. 16. The constant behaviour of frictional work density also starts at around 2.0°. At high loads, the differences between the inner ring raceway and the outer ring raceway are clear both for the frictional work density and for the maximum sliding path.

8. Discussion

In the following, the results of the simulations are discussed in relation to the derivation of a critical amplitude. The discussion is theoretically targeting complex relationships without simplification.

8.1. Definition of a critical amplitude θ_{crit}

The parameter study was carried out to clarify the question of whether the definition of a critical amplitude is possible under simplified conditions.

The analysis shows that the frictional work density is constant for $e > 1$. Between $e = 0.5$ and $e <= 1$, the frictional work density can be approximated with a second-order polynomial function. For $e < 0.5$, it is possible to approximate the frictional work with a linear function. Between $e = 0$ and $e < 1$ a polynomial function of second-order allows sufficient approximation.

The described behaviour of the frictional work density can be explained by the swept area and the distribution of the frictional work density (see Fig. 10 or Video). For $e < 1$, the frictional work's non-constant (polynomial) behaviour can be explained by the swept area, decreasing with increasing amplitudes and the distribution of the frictional work shown exemplarily in Fig. 17. Since the highest frictional work areas are within the swept area for $e < 0.5$, even a linear approximation is sufficient for such amplitudes. For $e > 1$ the accumulated frictional work is not affected by the swept area, which leads to the constant behaviour of the
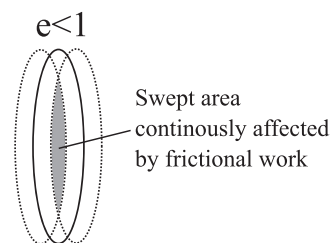

Fig. 17. Visualization of the swept area which is continuously affected by frictional work for $e < 1$.
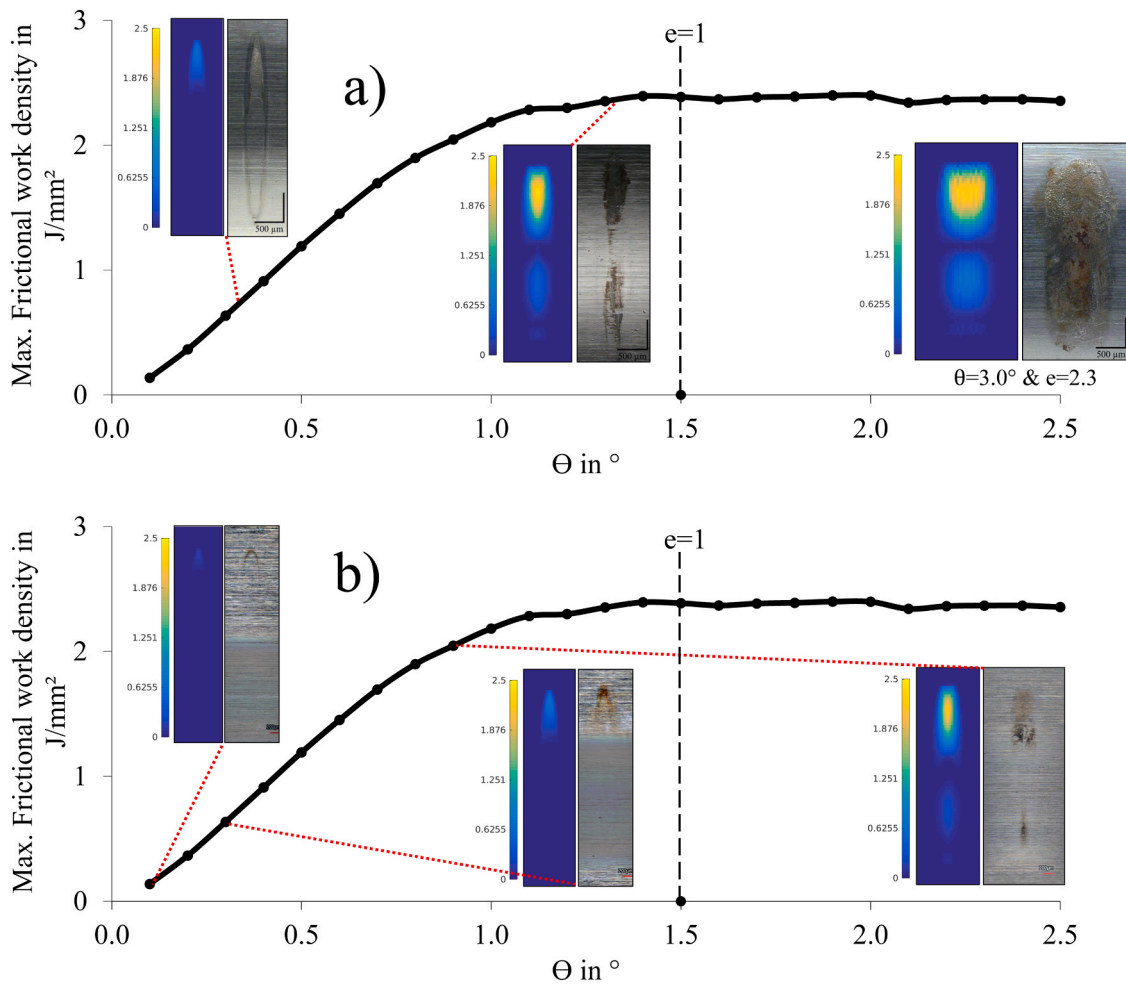
Fig. 18. Qualitative comparison of simulation results and experiments from Schwack et al. [57]. a) Experiments used grease lubricant [57], Table 3. b) Dry experiments [17].

Table 3
Grease properties.

NLGI	2
Thickener	Lithium
Base oil viscosity (40 °C)	50 mm^2/s
Base oil	Synthetic

frictional work with increasing amplitudes. This was shown for fretting contacts by Fouvry et al. [44] and is also in line with θ_{dith} from Harris et al. [35]. A critical amplitude can be derived for simplified conditions for an θ that corresponds to $e = 1$.

This relationship can be used to better understand the definition of a critical amplitude for certain parameter combinations. The amplitude no longer has any influence if e is greater than 1. This also means that for the aforementioned simplifications, there is no difference between oscillations with $e > 1$ and rotating bearings.

However, the application of rolling bearings is subject to more complex conditions. In particular, lubrication must be taken into account when defining a critical amplitude. The rule is that the greater the amplitude, the greater the chance that the lubricant can prevent wear. If lubrication cannot be guaranteed, the wear is much greater at large amplitudes, as can be seen in the experiments found in literature [22,23]. For lubricated bearings, both small and large amplitudes can lead to critical operating conditions that promote wear.

Fig. 18a shows a comparison of the simulation results and experiments

from Schwack [57]. The bearing size is the same for simulations and experiments. The bearings were lubricated with a grease commonly used in wind turbine pitch bearings (see Table 3) The experiments run around 100,000 oscillating cycles. It can be seen that the wear distribution corresponds to the frictional work density.

Fig. 18b shows a comparison of the simulation results and the experiments from Schwack et al. [17]. The bearings were used dry in this experiments and for less than 1000 cycles. For 1000 cycles, no wear occurs for grease lubricated bearings. Under dry conditions, such a low cycle count helps to compare the first signs of wear with the simulations.

8.2. Comparison to fretting

The contact/motion configurations most frequently employed in fretting research thus represent simplified and controlled fretting scenarios that allow for this form of detailed fundamental analysis to take place. Following that line of thought, the model employed in this work reveals that, despite all of the increased kinematic complexity of a rolling element bearing contact, an interesting parallel is found when contemplating the relationship of the swept contact area and the contact size to the resulting frictional work density. This model behaviour, of rising frictional energy density as the e-ratio increases towards a value of 1 and then remains constant for larger e values, is also shared by that of a tangentially loaded contact as described by Fouvry et al. [44].

8.3. Influence of coefficient of friction μ

The coefficient of friction μ depends from the used lubricant and the lubrication conditions. To promote understanding, a separation of friction and lubrication is sought in the course of the discussion, in which overlapping cannot be completely avoided.

The simulations made the simplified assumptions that the coefficient of friction μ is constant for all parameters in one simulation and that the coefficient of friction is constant in the contact zone. In order to find approximations for the model, literature can be used. In Lenart et al. [58] for example, coefficients of friction are given for dry contacts or in Schwack [57] tribometer measurements are carried out to determine the coefficient of friction for various lubricants.

The coefficient of friction may vary through a complete oscillation due to the varying speed of the rolling element. Furthermore, time-depended effect like changes of micro- and macro geometry as well as changing lubricant behaviour may influence μ as well. The presented model cannot take these influences into account. Nevertheless, the stated facts must be taken into account when interpreting and transferring the results.

In a lubricated bearing the coefficient of friction will be highly affected by the oscillating amplitude. For comparatively small amplitudes, the relative movements are too small to build up a lubricant film. How film thickness and amplitude ratio e interact can be seen in the ball-on-disc experiments by Maruyama et al. [21]. For an PAO oil, 411 mm^2/s at 40 °C viscosity, and a maximum contact pressure of 0.37 GPa it was shown, that for e below 1.6 no lubricant film establish. This result was independent of the vibrating speed. In the case of grease lubrication, the thickener can separate the contact surfaces. However, when the lubricant is not able to separate the contact surfaces, μ and therefore also the frictional work will reach high values. This is the main reason for wear under small amplitudes. Nevertheless, for the same μ, larger amplitudes will lead to higher frictional work density. It can be concluded that for larger amplitudes, the chance of adequate lubrication is higher due to the larger relative motion, but the larger relative movement also leads to more wear (compared to smaller amplitudes) if sufficient lubrication is not guaranteed.

9. Conclusion

The definition of a critical amplitude, which helps to identify wear-promoting operating conditions, is of great importance for the industrial applications of oscillating bearings since wear can be prevented without major changes to the system being necessary. We have therefore addressed the question of the critical amplitude with the help of simulations.

Based on a parametric study, which includes 125 simulations, in which different oscillating amplitudes θ, coefficients of friction μ and load conditions were varied, the following findings could be obtained:

- For oscillation amplitudes where the distance covered by the rolling element is smaller than the width of the Hertz'ian contact ($e < 1$), a linear increase between $e = 0$ and $e < 0.5$ and a polynomial increase between $e = 0.5$ and $e < =1$ for the frictional work density can be seen for increasing amplitudes. The coefficient of friction only mildly influences this ratio.
- For oscillation amplitudes that correspond to $e > 1$ a constant behaviour of the frictional work density was found. A further increase of the oscillating amplitude did not increase the frictional work.
- The relationship between e and the frictional work density also occurs for fretting investigation (single contact and pure sliding). Therefore, these results can help when transferring fretting experiments to bearing experiments.

All in all, a critical oscillating amplitude can be defined under simplified conditions. The critical oscillation amplitudes occur where the distance covered by the rolling element is smaller than the width of the Hertz'ian contact ($e < 1$).

CRediT authorship contribution statement

Fabian Schwack: Conceptualization, Methodology, Validation, Investigation, Data curation, Writing - original draft, Visualization, Project administration. **Volker Schneider**: Conceptualization, Methodology, Validation, Investigation, Data curation, Writing - original draft. **Sebastian Wandel**: Writing - original draft. **Román José de la Presilla**: Writing - original draft. **Sergei Glavatskih**: Supervision, Writing - review & editing. **Gerhard Poll**: Supervision, Writing - review & editing, Project administration, Funding acquisition.

Declaration of Competing Interest

The authors declare that they have no known competing financial interests or personal relationships that could have appeared to influence the work reported in this paper.

Appendix A. Supporting information

Supplementary data associated with this article can be found in the online version at doi:10.1016/j.triboint.2021.107154.

References

[1] Berthier Y, Play D. Wear mechanisms in oscillating bearings. Wear 1982;75: 369–87.
[2] Godfrey D. Fretting corrosion or false brinelling? Tribol Lubr Technol 2003;59: 28–9.
[3] Errichello R. Another perspective: false brinelling and fretting corrosion. Tribol Lubr Technol 2004;60:34–6.
[4] Vingsbo O, Söderberg S. On fretting maps. Wear 1988;1988:131–47.
[5] Brunnen A.J.D., Bentall R.H. Development of a high stability pointing mechanism for wide application, in: 16th Aerospace Mechanisms Symposium, NASA-CP-2221. 1982.
[6] Rogers LM. Detection of incipient damage in large rolling element bearings. Advanced materials research. vol. 13. Trans Tech Publ; 2006. p. 37–44.
[7] Wouter O, De Baets P, De Waele W. Failure of a large ball bearing of a dockside crane. Eng Fail Anal 2004;11:335–53.
[8] Kato M, Sato T. The development of low friction and anti-fretting corrosion greases for cvj and wheel bearing applications. SAE Trans 1987:1244–50.
[9] Lee CH, Choi JY, Jeon IS, Cho W, Yun H. Grease degradation in constant velocity (CV) joints. Tribol Trans 2011;54:825–31.
[10] Hlavacek I, Slama V, Najnar J. Zur Frage der durch an Textilmaschinen verursachten Schäden. Europäischer Tribologie Kongreß. Düsseldorf, Deutschland: Eurotrib; 1977.
[11] Mannens R, Trauth D, Falker J, Brecher C, Klocke F. Analysis of spindle bearing load with regard to the false brinelling effect caused by machine hammer peening. Int J Adv Manuf Technol 2018;95:3969–76.
[12] Fallahnezhad K, Liu S, Brinji O, Marker M, Meehan PA. Monitoring and modelling of false brinelling for railway bearings. Wear 2019;424:151–64.
[13] Almen JO. Lubricants and false brinelling of ball and roller bearings. Mech Eng 1937;59:415–22.
[14] Burton T, Sharpe D, Jenkins N, Bossanyi E. Wind energy handbook. 2 ed. London: Wiley & Sons; 2012.
[15] Hansen MOL. Aerodynamics of wind turbines. 3 ed. Routledge; 2015.
[16] Stammler M, Reuter A, Poll G. Cycle counting of roller bearing oscillations – case study of wind turbine individual pitching system. Renew Energy Focus 2018;25: 40–7.
[17] Schwack F, Prigge F, Poll G. Finite element simulation and experimental analysis of false brinelling and fretting corrosion. Tribol Int 2018;126:352–62.

[18] Grebe M. False Brinelling - standstill marks at roller bearings (Dissertation). Bratislava: Slovak University of Technology; 2012.

[19] Godfrey D. A study of fretting wear in mineral oil. Lubr Eng 1956;12:37–42.

[20] Schwack, F., Byckov, A., Bader, N., Poll, G. Time-dependent analyses of wear in oscillating bearing applications, in: 72th STLE Annual Meeting and Exhibition. 2017.

[21] Maruyama T, Saitoh T. Oil film behavior under minute vibrating conditions in EHL point contacts. Tribol Int 2010;43:1279–86.

[22] Schwack F, Bader N, Leckner J, Demaille C, Poll G. A study of grease lubricants under wind turbine pitch bearing conditions. Wear 2020:203335.

[23] Grebe M, Molter J, Schwack F, Poll G. Damage mechanisms in pivoting rolling bearings and their differentiation and simulation. Bear World J 2018;3:71–86.

[24] Grebe M, Feinle P, Hunsicker W. Einfluß verschiedener Faktoren auf die Entstehung von Stillstandsmarkierungen (False-BrinellingEffekt). Tribologie-Fachtagung, Göttingen: Deutschland, GfT; 2007.

[25] Grebe M, Feinle P, Hunsicker W. Möglichkeiten zur Reduzierung von False Brinelling Schäden. In: Tribologie-Fachtagung, Göttingen: Deutschland, GfT; 2008.

[26] Grebe M, Feinle P, Blaškovitš P. Failure of roller bearings without macroscopic motion - influence of the pivoting angle on the contact mechanics and the wear mechanisms in the contact between roller and raceway. Tribology - industrial and automotive lubrication. Ostfildern: Techn. Akad. Esslingen; 2014.

[27] Schadow C. Stillstehende fettgeschmierte Wälzlager unter dynamischer Beanspruchung (Dissertation). Magdeburg: Otto-von-Guericke-Universität; 2016.

[28] Deutsches Institut für Normung. DIN EN ISO 6506 - Metallische Werkstoffe - Härteprüfung nach Brinell, Beuth Verlag. 2015.

[29] El-Gamal HA, Awad TH. Optimum model shape of sliding bearings for oscillating motion. Tribol Int 1994;27:189–96.

[30] Kim NH, Won D, Burris D, Holtkamp B, Gessel GR, Swanson P, et al. Finite element analysis and experiments of metal/metal wear in oscillatory contacts. Wear 2005; 258:1787–93.

[31] Evans RD, Cooke EP, Ribaudo CR, Doll GL. Nanocomposite tribological coatings for rolling element bearings. Mater Res Soc Symp Proc 2002;750:407–17.

[32] Doll GL, Ribaudo CR, Evans RD. Engineered surfaces for steel rolling element bearings and gears. Mater Sci Technol 2004;2:367–74.

[33] Doll GL. Improving the performance of rolling element bearings with nanocomposite tribological coatings. SAE Tech Pap 2006.

[34] Eckels M, Kotzalas MN, Doll GL. Attaining high levels of bearing performance with a nanocomposite diamond-like carbon coating. Tribol Trans 2013;56:410–6.

[35] Harris T., Rumbarger J.H, Butterfield C.P Wind Turbine Design Guideline DG03: Yaw and Pitch Rolling Bearing Life: Technical Report, NREL/TP-500–42362, NREL. 2009.10.2172/969722.

[36] Juettner M, Hasse A, Tremmel S. Flexure pitch bearing concept for individual pitch control of wind turbines. Wind Energy 2018;21:129–38.

[37] Maruyama T, Saitoh T, Yokouchi A. Differences in mechanisms for fretting wear reduction between oil and grease lubrication. Tribol Trans 2017;60:497–505.

[38] McColl IR, Ding J, Leen SB. Finite element simulation and experimental validation of fretting wear. Wear 2004;256:1114–27.

[39] Brinji O, Fallahnezhad K, Meehan PA. Analytical model for predicting false brinelling in bearings. Wear 2019:203135.

[40] Fallahnezhad K, Brinji O, Desai A, Meehan PA. The influence of different types of loading on false brinelling. Wear 2019;440:203097.

[41] Cubillas D, Olave M, Llavori I, Ulacia I, Larrañaga J, Zurutuza A, et al. Numerical analysis of the wind turbine pitch bearing raceway tribo-contact due to cyclic loading under constant pitch angle. Fracture, fatigue and wear. Springer; 2020. p. 757–69.

[42] Krause H, Poll G. Wear of wheel-rail surfaces. Wear 1986;113:103–22.

[43] Liu Y, Xu JQ, Mutoh Y. Evaluation of fretting wear based on the frictional work and cyclic saturation concepts. Int J Mech Sci 2008;50:897–904.

[44] Fouvry S, Liskiewicz T, Kapsa Ph, Hannel S, Sauger E. An energy description of wear mechanisms and its applications to oscillating sliding contacts. Wear 2003; 255:287–98.

[45] Yue T, Wahab MA. Finite element analysis of fretting wear under variable coefficient of friction and different contact regimes. Tribol Int 2017;107:274–82.

[46] Jones AB. Ball motion and sliding friction in ball bearings. J Basic Eng 1959;81: 1–12.

[47] Leblanc A, Nelias D. Ball motion and sliding friction in a four-contact-point ball bearing. J Tribol 2007;129:801–8.

[48] Johnson KL. Contact mechanics. Cambridge: Cambridge University Press; 1985. https://doi.org/10.1017/CBO9781139171731.

[49] Heathcote HL. The ball bearing: In the making, under test and on service. Proc Inst Automob Eng 1920;1:569–702.

[50] Bisson EE, Anderson WJ. Advanced bearing technology. National Aeronautics and Space Administration, Scientific and Technical Information Office; 1964.

[51] Hamrock BJ. Rolling-element Bearings. vol. 1105. National Aeronautics and Space Administration, Scientific and Technical Information Office; 1983.

[52] Hertz HR. Über die berührung fester elastischer körper. J Reine Angew Math 1881; 92:156–71.

[53] Stammler M, Thomas P, Reuter A, Schwack F, Poll G. Effect of load reduction mechanisms on loads and blade bearing movements of wind turbines. Wind Energy 2020;23:274–90.

[54] Stolarski T, Nakasone Y, Yoshimoto S. Engineering analysis with ANSYS software. Butterworth-Heinemann; 2018.

[55] Fouvry S, Paulin C. An effective friction energy density approach to predict solid lubricant friction endurance: application to fretting wear. Wear 2014;319:211–26.

[56] Schwack F, Stammler M, Flory H, Poll G. Free contact angles in pitch bearings and their impact on contact and stress conditions. Hamburg: European Wind Energy Association; 2016.

[57] Schwack F. Untersuchungen zum Betriebsverhalten oszillierender Wälzlager am Beispiel von Rotorblattlagern in Windenergieanlagen (Ph.D. thesis). Leibniz Universität Hannover; 2020.

[58] Lenart A, Pawlus P, Dzierwa A, Sep J, Dudek K. The effect of surface topography on dry fretting in the gross slip regime. Arch Civ Mech Eng 2017;17:894–904.